Egress of human cytomegalovirus through multivesicular bodies

Felix J. Flomm[1,2,3,4], Timothy K. Soh[1,2,3,4], Carola Schneider[4], Hannah M. Britt[5], Konstantinos Thalassinos[5,6], Søren Pfitzner[4], Rudolph Reimer[4], Kay Grünewald[1,3,4,7], Jens B. Bosse[1,2,3,4]*

[1] Centre for Structural Systems Biology, Hamburg, Germany
[2] Hannover Medical School, Institute of Virology, Hannover, Germany
[3] Cluster of Excellence RESIST (EXC 2155), Hannover Medical School, Hannover, Germany
[4] Leibniz-Institute for Experimental Virology (HPI), Hamburg, Germany
[5] Institute of Structural and Molecular Biology, Division of Biosciences, University College London, London, United Kingdom
[6] Institute of Structural and Molecular Biology, Birkbeck College, University of London, London, United Kingdom
[7] University of Hamburg, Department of Chemistry, Hamburg, Germany

*Jens B. Bosse, Center for Structural Systems Biology, Notkestraße 85, 22607 Hamburg

Corresponding Author Email: jens.bernhard.bosse@cssb-hamburg.de

Author ORCIDs

Felix J. Flomm: 0000-0001-7691-0519

Hannah M. Britt 0000-0001-8510-0331

Konstantinos Thalassinos 0000-0001-5072-8428

Søren Pfitzner 0000-0002-0155-0317

Kay Grünewald: 0000-0002-4788-2691

Jens B. Bosse: 0000-0001-7252-5541

Keywords

Human cytomegalovirus, Integrative microscopy, Viral egress, Morphogenesis

Author Contributions

Designed research: FJF, KT, RR, KG, JBB; Performed research: FJF, TKS, CS, HB, RR; Contributed new analytic tools: RR, CS, SP; Analyzed data: FJF, TKS, JBB; Wrote the paper: KG, FJF, TKS, JBB.

Abstract

Human Cytomegalovirus (HCMV) can infect a variety of cell types by using virions of varying glycoprotein composition. It is unclear how this diversity is generated, but spatiotemporally separated envelopment and egress pathways might play a role. So far, one egress pathway has been described in which HCMV particles are separately enveloped into individual vesicles and

continuously exocytosed. However, some studies have also found enveloped virus particles inside multivesicular bodies (MVBs) but could not link them to productive egress or degradation pathways. We used a novel 3D-CLEM workflow to investigate MVBs in HCMV morphogenesis and egress. We found that HCMV envelopment occurred at MVBs and that virus-filled MVBs traversed the cytoplasm to release virions in bulk at the plasma membrane to form extracellular virus accumulations. Our data support the existence of a novel bona fide HCMV egress pathway, which opens the gate to evaluate divergent egress pathways in generating virion diversity.

Introduction

Human Cytomegalovirus (HCMV) is a ubiquitous betaherpesvirus of high clinical importance that establishes lifelong latent infection in humans. It is the leading cause of congenital disabilities in the developed world and a significant cause of disease in immunocompromised patients, such as transplant, AIDS, or cancer patients (reviewed in (Griffiths, 2020)). It has been ranked highest priority for vaccine development by the Institute of Medicine for over 20 years (Modlin et al., 2004). Still, despite continuing efforts, no licensed vaccine exists so far, and antiviral therapy currently is the only management option with the development of viral resistance being a significant concern (Britt and Prichard, 2018). As HCMV causes disease affecting various tissue types and organs, understanding how HCMV can infect different cell types is essential for developing novel antiviral strategies.

HCMV infected cells release distinct virus populations that differ in their glycoprotein content (Adler, 2015; Scrivano et al., 2011) to target specific cell types. While the pentameric complex consisting of gH/gL/UL128/pUL130/pUL131 guides tropism for endothelial and epithelial cells, especially through cell-to-cell spread, the trimeric complex consisting of gH/gL/gO is needed to mediate infectivity of cell-free virions. Factors that mediate the abundance of these complexes on virions have been recently identified (Adler, 2015; Bronzini et al., 2012; Li et al., 2015; Luganini et al., 2017; Nguyen et al., 2018), but it is unclear how distinct glycoprotein concentrations on individual particles are achieved. Spatiotemporally separated envelopment or egress pathways could explain how distinct virus populations are generated, but little is known about these aspects of HCMV assembly.

Herpesviruses virions assemble in the host cytoplasm using a culminating step called secondary envelopment. During secondary envelopment, viral capsids bud into host-derived membranes, resulting in enveloped viral particles inside transport vesicles (reviewed in (Johnson and Baines, 2011; Owen et al., 2015). These transport vesicles subsequently release mature virions by fusing with the plasma membrane. Compared to the morphogenesis of the alphaherpesviruses, e.g. herpes simplex virus 1 (HSV-1) and pseudorabies virus (PRV), HCMV morphogenesis is much more involved, taking not hours but several days. During this time, the virus extensively remodels the host cell's secretory apparatus leading to the formation of the assembly compartment (AC) (Sanchez et al., 2000). The AC is a dense, donut-shaped, perinuclear structure consisting of convoluted and interconnected membranes which are centered around the microtubule-organizing center (Procter et al., 2018). It contains many cellular proteins traditionally used as organelle specific markers, including proteins originally associated with Golgi, trans-Golgi, endosomes, and lysosomes (Cepeda et al., 2010; Das and Pellett, 2011; Das et al., 2007; Homman-Loudiyi et al., 2003). However, the extensive viral transformation of the cell´s secretory pathways during AC formation and the short-circuiting of established cellular pathways through viral factors is making the origin of membranes and their identity less clear. Consistently, proteomics indicate that the virus-induced reorganization of the secretory apparatus during AC formation mixes membranes from different sources as targets for secondary envelopment (Moorman et al., 2010; Turner et al., 2020).

Currently, capsid secondary envelopment events have been only shown to occur as individual events at small vesicles in the center of the AC (Schauflinger et al., 2013; Taisne et al., 2019). This is insofar consistent with data from alphaherpesviruses where individual virions are continuously released through the fusion of diffraction-limited exocytic vesicles with the plasma membrane (Hogue et al., 2014; Hollinshead et al., 2012). However, other studies also found enveloped HCMV

particles in large structures resembling multivesicular bodies (MVBs) of unknown origin (Bughio et al., 2015; Homman-Loudiyi et al., 2003; Schauflinger et al., 2011; Tooze et al., 1993) but secondary envelopment or subsequent release into the extracellular space could not be shown at them. Therefore, it is currently unclear if virus particles in MVBs indicate a productive egress pathway or are targeted for degradation. Interestingly, it has been shown that deleting the viral protein UL135 leads to an abrogation of virus-filled MVBs, and mutating UL71, another viral protein, leads to an enlargement of these MVBs (Schauflinger et al., 2011), possibly indicating a productive role. In addition, a number of other publications implicate MVBs in HCMV morphogenesis (Bughio et al., 2013, 2015; Dietz et al., 2018; Meissner et al., 2012; Schauflinger et al., 2011) and data from the related human herpesvirus 6A (HHV-6A) suggest MVB-like structures as targets for egress (Mori et al., 2008).

To provide an unbiased view on HCMV envelopment and identify potential alternative HCMV egress routes, we employed an integrative approach based on volumetric live-cell imaging and three-dimensional correlative light and electron microscopy (3D-CLEM). It provided an unprecedented, spatiotemporally highly resolved views into whole HCMV infected cells. Unexpectedly, we found large transient accumulations of enveloped virions in MVB-like structures that we dubbed virus-containing MVBs (vMVBs) as well as clustering at the plasma membrane in extracellular viral accumulations (EVAs). Importantly, we found secondary envelopment events at vMVBs, strongly suggesting that they are bona fide targets of the viral envelopment machinery. Live-cell lattice light-sheet microscopy (LLSM) showed that vMVBs were transported to the plasma membrane, where they relaxed and distributed their viral contents. A pH-sensitive biosensor confirmed that these relaxation events were indeed membrane fusion events. Our data argue for a model in which a large fraction of HCMV capsids envelope at vMVBs, which subsequently are transported to the plasma membrane where they fuse intermittently and release bulk pulses of viral particles. This pathway likely constitutes a so-far neglected HCMV egress route. Future work should dissect its role in generating virion diversity.

Results

HCMV-infected fibroblasts accumulate viral material at specific extracellular sites

To get an overview of HCMV envelopment and egress routes, we initially used live-spinning disk fluorescence microscopy and followed the fate of capsids and viral membranes with an HCMV mutant expressing EGFP-labeled capsid-associated tegument protein pp150 and mCherry-labeled glycoprotein gM (HCMV-TB40-pp150-EGFP-gM-mCherry) (Sampaio et al., 2013) using single-particle tracking. Despite considerable effort and computational filtering of thousands of analyzed capsid tracks, we were unable to identify more than a few events in which diffraction-limited capsid and membrane signals merged and were co-transported subsequently. While we assumed that this was due to the high signal background in the viral AC, it made us look for alternative HCMV egress envelopment and routes that we missed by focusing on trackable small individual events.

Surprisingly, we found that between 72 and 96 hpi pp150-EGFP and gM-mCherry positive virus material accumulated at specific sites in the extracellular space below the cell, similar to exocytosis hotspots that have been described for HSV-1 (Mingo et al., 2012) (Fig. 1C). We dubbed these extracellular viral accumulations (EVAs). At 120 hpi 80-90% of late-infected cells had EVAs at their plasma membrane (Fig. 1B).

To investigate the nature and genesis of EVAs in HCMV-infected human foreskin fibroblasts, we developed a novel three-dimensional correlative light and electron microscopy (3D-CLEM) workflow that combines spinning disk fluorescence microscopy with serial block-face scanning electron microscopy (SBF-SEM). This approach allowed us to correlate specific labels for capsids (pp150) and viral membranes (gM) (Fig. 1A) with volumetric EM data of whole infected cells at high resolution.

We identified EVAs below infected cells by fluorescence microscopy (Fig. 1C) and analyzed them by 3D-CLEM (1D-F, Sup. Vid. 1). We found that infected cells accumulated virions, dark stained enveloped bodies (putative dense bodies) and a plethora of vesicles of different sizes in pp150 and

gM positive sites (Fig. 1B-F). We also observed large invaginations at the plasma membrane that might be the result of either endo- or exocytosis of EVAs (two slices from a volume are shown in Fig. 1F).

HCMV particles bud into and accumulate in MVBs

Next we sought to investigate the source of EVAs. To our surprise, we also found large intracellular bodies positive for both capsid and viral membrane markers at four days post-infection (dpi). A z-projection of a 3D spinning-disc-microscopy stack from two adjacent cells is shown in Fig. 2B, and a merge of the light and electron microscopy data in Fig. 2C illustrates the correlation of the datasets. Correlation and volume rendering of the large pp150 and gM positive spots in the fluorescence data in the EM volume confirms that these are closed multivesicular structures filled with significant numbers of virions, dense bodies as well as other structures (Fig. 2E-H) that we dubbed virus-containing multivesicular bodies (vMVBs). The 3D rendering (Fig. 2F) illustrates their large extension in the z-direction. The vMVBs in our data resembled structures described in other studies (Bughio et al., 2013; Schauflinger et al., 2011) but it had been unclear if they are the result of a so-far unrecognized egress pathway or a degradation pathway. Using the full volumetric data, we found non-enveloped particles budding into MVBs, indicating that the MVBs were a target for de novo HCMV secondary envelopment (Fig. 2G-H, Sup. Fig. 3). vMVBs were very heterogeneous in size and content. Some contained only a few particles, others up to several hundred (see also Sup. Fig 1 for an overview of a complete AC). Smaller virus-containing vesicles described in previous EM-based studies (Schauflinger et al., 2013) were often not as obvious in fluorescence microscopy but could also be found in the SBF-SEM data (Sup. Fig. 2). We also regularly found vMVBs in cells infected with wild-type HCMV (Sup. Fig. 4).

Pulses of bulk release lead to viral extracellular accumulations at the plasma membrane

To illuminate the fate of vMVBs, we used two modalities of live-cell fluorescence microscopy. First, we utilized inverted lattice light-sheet microscopy to acquire 3D-volumes of infected cells at high temporal resolution for 15-45 minutes with minimal phototoxicity and photobleaching. We found that vMVBs traveled from the assembly complex to the plasma membrane, where they seemed to relax, possibly indicating their fusion with the plasma membrane (Fig. 3B, Sup. Vid. 3). In a second approach, we imaged longer timespans in the infection cycle using time-lapse live-cell microscopy with less temporal coverage in 2D. To this end, we used a modified HCMV mutant with more photostable fluorescent tags (HCMV-TB40-pp150-SNAP-gM-mScarlet-I) for imaging z-stacks over several days. We imaged HFF cells between 72 and 96 hpi for 18 to 60 hours every 40 minutes with a spinning-disc-confocal fluorescence microscope. Strikingly, we observed vMVBs coming close to the observation plane which was focused near the plasma membrane where they relaxed into patches of viral material, which resembled the EVAs shown in Fig. 1. These EVAs were positive for pp150 and gM and did not diffuse away. EVAs seemed to also attach to the growth support since they were left behind when cells moved away. EVA formation generally occurred as intermittent pulses as vMVBs came into the observation plane near the plasma membrane and relaxed (Fig. 3C, Sup. Vid. 4-5). Release events varied in fluorescence intensity, which is consistent with our observation that vMVBs were very heterogeneous in size and content.

vMVBs release their cargo through fusion with the plasma membrane and result in EVAs

To confirm that the observed bulk release events were indeed induced by fusion with the plasma membrane, we used the pH-sensitive fluorescent protein super-ecliptic pHluorin as a biosensor to detect exocytosis events. We created a cell line stably expressing a CD63-pHluorin fusion construct (Bebelman et al., 2020) as our data indicated that CD63 is enriched on vMVBs membranes but not on virions. In this construct, pHluorin is inserted into an extracellular loop of CD63, such that it points towards the luminal side in multivesicular structures and to the extracellular environment after fusion. Accordingly, pHluorin is quenched by the acidic pH inside this luminal space of MVBs,

rendering the construct almost non-fluorescent. However, upon fusion with the plasma membrane, pHluorin gets exposed to the pH-neutral extracellular milieu, and fluorescence recovers rapidly. The increase in fluorescence intensity provides an easily detectable and quantifiable indicator of fusion with the plasma membrane. Imaging of fixed, permeabilized cells in which intracellular pHluorin was dequenched, confirmed that the fluorescence signal from the CD63-fusion marked gM and gB positive bodies (Sup. Fig. 5A-C).

For imaging of potential fusion events, we picked cells that had not yet accumulated EVAs on the outside of the basolateral cell surface and used live-cell total internal reflection microscopy (TIRF) to image fusion events for several hours without phototoxicity. We took images every 1.5-2 seconds for 60 minutes since we predicted that actual membrane fusion and pH equilibration might be very rapid. We found that vMVBs came into the TIRF-field and relaxed into EVAs shortly after arrival at the plasma membrane and resulting in EVAs positive for pp150 and gM (Fig. 4B, arrows). Strikingly, these events were accompanied by flashes of green fluorescence between the vMVBs arrival and the relaxation event, indicating that membranes had fused (Fig. 4C). The rapid reduction of green fluorescence indicated that CD63 quickly diffused away from the fusion site. The gM signal increased directly before the fusion event and decreased as vMVBs relaxed into a flattened patch. The exocytosed material emitted a continuously elevated signal. These results are consistent with CD63 not being incorporated into virions (Fig. 5). The transition from vMVBs to EVAs took much longer than the actual fusion event, suggesting that fusion pore expansion and cargo expulsion were slow.

vMVBs carry markers of the endocytic trafficking system and the exosome pathway

Intermittent bulk release of vesicles is a functional hallmark of exosomal pathways. Therefore, we used immunofluorescence combined with mass spectrometry to approximate possible overlaps between virus composition and exosome generation. To this end, we performed a mass spectrometry analysis of gradient-purified extracellular virions. Gradient-purified virus particles contained markers of Golgi-to-endosome trafficking (syntaxin 12, Rab14, VAMP3), early endosomes (Rab 5C, syntaxin 7), as well as exosomes (HSP70, HSP90, GAPDH, enolase 1, 14-3-3, and PKM2), suggesting that HCMV might use a mix of membranes originally originating from Golgi- and endosomal membranes for secondary envelopment to generate vMVBs (Sup. Table 1). Our findings are consistent with a recent study by Turner et al., concluding that HCMV hijacks parts of the exosome pathway for egress (Turner et al., 2020).

Other classical markers for membranes used in the exosomal pathway are the tetraspanins CD9, CD63, and CD81. CD63 has been investigated in the context of HCMV infection before, however, with conflicting results (Hashimoto et al., 2020; Streck et al., 2020). Using immunofluorescence, we tested if they are localized to vMVBs. The density of protein signals in the AC complicated analysis, but we found CD63 colocalizing with large vesicles also containing pp150 and gM (Fig. 5B-D) while CD9 and CD81, in our hands, localized to the AC but not specifically to vMVBs (Sup. Fig. 6A-B). On the other hand, exocytosed material in EVAs did not show any CD63, implying that CD63 is unlikely to be incorporated into virions (Fig. 5A-C). This observation is supported by the absence of CD63 in our virion proteomics data (Sup. Tab. 1) and in line with previous studies (Varnum et al., 2004).

Discussion

Little data exist on the spatiotemporal organization of HCMV egress at the subcellular level. Previous studies have mostly reported single-virion/single-vesicle envelopment events, which have shaped our current picture of HCMV secondary envelopment (Schauflinger et al., 2011, 2013). These data are consistent with a study by Hogue et al. (Hogue et al., 2016), which shows that individual alphaherpesvirus virions are released at the plasma membrane. Still, data suggests that virus-filled MVBs can form in HCMV-infected cells as well as HHV-6A and MCMV infected cells

(Bughio et al., 2013; Homman-Loudiyi et al., 2003; Maninger et al., 2011; Mori et al., 2008; Schauflinger et al., 2011) and that Golgi- and endosome-derived membranes are targeted by HCMV (Cepeda et al., 2010; Das and Pellett, 2011; Das et al., 2007; Homman-Loudiyi et al., 2003; Tooze et al., 1993; Varnum et al., 2004). However, a functional role for vMVBs in egress has lacked so far (Bughio et al., 2015; Homman-Loudiyi et al., 2003; Schauflinger et al., 2011; Tooze et al., 1993) and it was unclear if vMVBs are part of a productive egress pathway.

Here, we were intrigued by the occurrence of EVAs in the majority of infected cells and investigated their formation. We found that HCMV can form virus particles by budding into vMVBs by using a novel 3D-CLEM workflow that combines dynamic information from spinning disk fluorescence microscopy with high-resolution information from serial block-face scanning electron microscopy. Using time-lapse and functional live cell imaging, we provided evidence that suggests that vMVBs can fuse with the plasma membrane and intermittently release tens to hundreds of virus particles in bulk, resulting in plasma membrane-associated EVAs. Importantly, quantification of EVA prevalence in late infected cells suggested that they are not a rare phenotype but occur frequently in HCMV infection. Finally, proteomics of purified virions, functional imaging, and correlation of CD63 with vMVBs suggested that vMVB-mediated HCMV egress might use features of the cellular exosomal pathway.

Our live-cell imaging indicates that vMVBs form relatively quickly between 72 and 96 hpi and are soon released asynchronously, leading to pulses of EVA formation. This mechanism is in contrast to studies which have been performed in alphaherpesviruses, where single PRV virus particles have been shown to travel to the plasmamembrane and be released by fusion (Hogue et al., 2014). Our data however, does not exclude the existence of a separate egress pathway analogue to the mechanisms shown for alphaherpesviruses (reviewed in (Hogue, 2022)). Compared to previous studies, our new correlative 3D-CLEM workflow provides a major technological advancement as it permits us to observe whole cells in a defined infection state with less effort compared to precise but tedious serial sectioning (Schauflinger et al., 2013). This has allowed us to analyze transient vMVBs, which would have been otherwise hard to catch at high resolution.

It is unclear if the virus uses bona fide cellular MVBs for envelopment and transforms them into vMVBs or if they are generated *de novo*. Cellular MVBs produce similar bulk pulses of extracellular vesicles (EVs) or exosomes by fusing with the plasma membrane (Cocucci et al., 2009; Colombo et al., 2014; Théry et al., 2002). EVs form through inward budding at late endosomes. This process generates MVBs characterized by the presence of the late endosomal markers CD63, LAMP1, LAMP2, Rab4, and Rab5 (reviewed in (Colombo et al., 2014)). Budding at MVBs is catalyzed by the endosomal sorting complex required for transport (ESCRT) (Colombo et al., 2014). While some parts of the ESCRT machinery play a role in the secondary envelopment of alphaherpesviruses (Butt et al., 2020; Crump et al., 2007; Kharkwal et al., 2014; Pawliczek and Crump, 2009), they likely do not play a role in HCMV infection (Fraile- Ramos et al., 2007; Streck et al., 2018; Tandon et al., 2009). However, it was recently shown that HSV-1 proteins pUL7 and pUL51 form a complex that might constitute a mimic of an ESCRT-III complex. HCMV homologs pUL103 and pUL71 are predicted to be structurally very similar to their HSV-1 counterparts and might likewise perform ESCRT functions for the virus during infection (Butt et al., 2020). A recent proteomics study might support this notion by showing that HCMV utilizes parts of the exosome biogenesis machinery independently of classical ESCRT-pathways (Turner et al., 2020).

Members of the tetraspanin family, such as CD9, CD81, and CD63, have also been described to be enriched on EV membranes (Théry et al., 2002). Tetraspanins are known to form microdomains called tetraspanin-enriched microdomains on the cell surface (Yáñez-Mó et al., 2009) and are active in the organization of the plasma membrane, recycling, and cellular signaling (Takino et al., 2003; Yáñez-Mó et al., 2009). Tetraspanins are involved in sorting and targeting cargo to MVBs and, in cooperation with the ESCRT machinery, into EVs (Perez-Hernandez et al., 2013; van Niel et al., 2011). While it has been shown that HCMV-infected cells release EVs that contain viral surface proteins such as gB (Zicari et al., 2018), the role of exosomal pathways in HCMV particle envelopment and release are broadly not defined. Although inhibitors of exosome biogenesis can slow HCMV spread, they do not seem to have a significant influence on viral titers (Kosaka et al.,

2010; Streck et al., 2020), possibly arguing for an involvement of the MVB/exosome-pathways in cell-to-cell spread. Contradictory evidence exists for the role of CD63 in HCMV virus production. While one study does not find a significant effect of siRNA-mediated CD63 knockdown on HCMV titers (Streck et al., 2020) another recent study finds a substantial reduction of HCMV titers upon CD63 siRNA knock-down (Hashimoto et al., 2020).

We found colocalization between the tetraspanin CD63 and gB, gM, and pp150. However, CD81 and CD9, which are also associated with exosomes, did not, in our hands, colocalize with the viral markers as strongly. Since EVAs were negative for CD63, this marker might be excluded during the budding process at the MVB surface. CD63 possibly plays a role in the sorting of viral glycoproteins to sites of secondary envelopment, as tetraspanins are known to be involved in sorting plasma membrane-bound molecules into MVBs (Perez-Hernandez et al., 2013; van Niel et al., 2011). HCMV gB is known to localize to the plasma membrane and be sorted through endocytic and recycling pathways by an acidic cluster in its cytoplasmic domain (Radsak et al., 1996; Tugizov et al., 1999). For HSV-1, it was reported that disrupting the endosome-to-MVB trafficking pathway leads to mislocalization of the HSV-1 gB (Calistri et al., 2007). More recently, it has also been reported that HSV-1 replication leads to an increase of exocytosis of CD63 with extracellular vesicles, leading the authors to hypothesize that HSV-1 modulates exosome biogenesis for its benefit (Dogrammatzis et al., 2018). Taken together, these reports indicate that endocytic pathways can be involved in the trafficking of viral factors to sites of herpesvirus secondary envelopment. Our observation that HCMV gB strongly localized with CD63 might support this hypothesis and fits a recent report that gB is enriched in exosomes (Zicari et al., 2018). Moreover, a recent proteomics study focusing on exosome release from HCMV infected cells is in line with this interpretation (Turner et al., 2020). This study was able to further identify several additional viral proteins that likewise appear in exosomes. The data provided by the authors strengthens the overall idea that HCMV exploits endocytic trafficking and exosome biogenesis pathways for the assembly and egress of virus particles.

Alternatively, vMVBs might originate from the fusion of individual virus-filled transport vesicles as described for the related betaherpesvirus HHV-6A (Mori et al., 2008). This model fits reports that MVBs were mostly found in the AC periphery while most capsid budding into individual vesicles is observed in the center of the AC, where early endosomal markers and Golgi-markers merge (Das and Pellett, 2011; Das et al., 2007). However, in the work we present here, we regularly found budding events at MVBs but could not identify intracellular vesicle fusion events leading to vMVB formation in full 3D-EM volumes. We, therefore, conclude that vMVB-mediated HCMV egress is a novel spatiotemporally separated egress pathway.

HCMV produces cell-free virus in addition to cell-associated virus in fibroblasts and predominantly cell-associated progeny in endothelial cells (Scrivano et al., 2011). These different particle populations vary in their trimeric to pentameric glycoprotein complex composition and cell tropism. It is plausible to hypothesize that these virus populations might undergo different envelopment processes in the cell and are exocytosed with a different spatiotemporal profile (Scrivano et al., 2011). While this manuscript was in preparation, a study from the Wilson and Goodrum lab suggested that virus-containing MVBs in fibroblasts and endothelial cells are derived from different cellular membranes, which would add another potential HCMV egress pathway that could result in different virus populations; however, it is unclear if these pathways are functional in egress (Momtaz et al., 2021).

Future work needs to focus on characterizing the particle populations that are exocytosed by these pathways with regards to their glycoprotein content and define their role in potentially divergent egress routes. We used the HCMV strain TB40, which can produce two virus populations on HFF cells that are endothelial-cell and fibroblast-topic (Scrivano et al., 2011). The EVAs that we found were largely static during live-cell imaging and might represent a cell-associated viral population. We found EVAs not only trapped between the cell and the cell support but also on the upper side of infected cells, as well as between cells which would support the idea of cell-to-cell spread. However, our proteomics data, as well as a recent study (Turner et al., 2020), found that soluble, purified virions showed markers of the exosome pathway. If the virions released through EVAs are

the only ones that carry exosome-markers, then this would suggest that it is unlikely that they stay cell-associated and play a role in cell-to-cell spread.
In summary, our data, combined with published studies, suggest a model in which membranes originating from a fusion of both the endosomal and trans-Golgi network are used for either individual envelopment or capsids or to generate vMVBs in spatiotemporally separated processes. vMVBs are then transported to the plasma membrane, where fusion results in bulk pulses of virus particle exocytosis and formation of EVAs (Fig. 6).

Materials and Methods

Cells and Viruses

HFF-1 cells (ATCC-SCRC-1041, ATCC) were cultivated in Dulbecco's Modified Eagles Medium Glutamax (Thermo Fisher Scientific), supplemented with 5% FBS superior (Merck) and $2*10^5$ units/ml Recombinant Human FGF-basic (PeproTech Inc.). HCMV-pp150-EGFP-gM-mCherry was a kind gift by Christian Sinzger (Sampaio et al., 2013). The HCMV-TB-40-BAC4 was a kind gift by Wolfram Brune (Sinzger et al., 2008).

Spinning Disk Fluorescence Microscopy

Spinning disk microscopy was carried out on a Nikon TI2 (Nikon) based spinning disk system equipped with a Yokogawa W2, a Nikon 1.49 NA Apo-TIRF objective, and an Andor iXON888 EMCCD (Andor Technology). The resulting pixel size was 130nm, and image acquisition was done with NIS-Elements. Further, the setup was equipped with 405, 488, 561, and 640 laser lines and corresponding filter sets. Life cell experiments were carried out with a humidified incubation chamber heated to 37°C and 5% CO2 controlled by a gas mixer. For fluorescence microscopy, cells were grown in Ibidi 35mm glass-bottom dishes (Ibidi GmbH), for CLEM in Ibidi 35mm grid polymer bottom dishes. SNAP labeling before live-cell imaging with SNAP-Cell 647-SIR (New England Biolabs GmbH) was done according to the manufacturer's instructions. Image processing and analysis were performed in ImageJ/FIJI.

Serial Block Face Scanning Electron Microscopy (SBF-SEM)

For SBF-SEM, cells were fixed at the indicated time-points with 2% Paraformaldehyde (PFA/ Science Services) and 2.5% Glutaraldehyde (GA/ Science Services GmbH) in Dulbecco's phosphate-buffered saline (D-PBS, Sigma-Aldrich) for 5 minutes at room temperature (RT) and 55 minutes on ice. Subsequently, the sample was processed with the following procedure: Postfixation with 2% Osmium Tetroxide (OsO_4/ Science Services) and 2.5% GA in D-PBS on ice, staining with 2% OsO_4, 1.5% potassium ferrocyanide (Sigma-Aldrich), 2mM $CaCl_2$ (Sigma-Aldrich) in water, incubation in 0.5% thiocarbohydrazide (Sigma-Aldrich) in water, staining with 2% OsO_4 in water, incubation in 1% gallic acid (Sigma-Aldrich) in water, staining with 2% uranyl acetate (Merck KGaA) overnight in water. On the next day, the sample was stained with freshly prepared Waltons lead aspartate (Walton, 1979) ($Pb(NO_3)_2$ (Carl-Roth), L-Aspartate (Carl-Roth), KOH (Merck)), and subsequently subjected to a PLT dehydration series to Ethanol Rotipuran (Carl-Roth). Finally, the samples were infiltrated with 70% Epon in Ethanol before two incubations with 100% Epon and the final polymerization was carried out in Epon supplemented with 3% silver flakes (Sigma-Aldrich) and 3% (w/w) Ketjen Black (TAAB). Sample blocks of 0.5x0.5 mm were cut, mounted, and inserted into a Gatan 3View stage (Gatan) built in a Jeol JSM-7100F scanning electron microscope (Jeol). For imaging, the sample stage was biased with a 500V positive charge to account for sample charging during the scanning process. For the acquisition, 3x3 nm pixel size images were scanned, followed by the repeated ablation of 50 nm sections. The acquisition was controlled by the Gatan Digital Micrograph software, which was also used for stack alignments. Further processing of the datasets was performed in FIJI, and the volumes were rendered in Imaris 8 (Bitplane).

Transmission Electron Microscopy (TEM)

For TEM, cells were fixed and processed as described for SBF-SEM up to the embedding step. The cells were embedded in Epon without fillers, sectioned to 50 nm on a Leica Ultracut Microtome, (Leica), and subsequently transferred to copper mesh grids. Electron microscopy was performed on an FEI Tecnai G20 (FEI/ Thermo Fisher Scientific) and images were acquired on an Olympus Veleta side mounted camera (Olympus).

Lattice Light Sheet Microscopy

Lattice light-sheet microscopy was performed on a Zeiss Lattice Light Sheet 7 (Carl Zeiss) as part of an early adaptor program, controlled with Zeiss Zen Blue software. The device is equipped with 488, 561, and 640 laser lines and multi-bandpass filters. Live-cell experiments were carried out on Ibidi 35mm glass-bottom dishes at 37°C with 5% CO2 in a humidified atmosphere. The acquisition was done on a pco.edge (PCO AG) sCMOS camera with a final pixel size of 145nm. Images were deconvolved after acquisition in Zen Blue using the built-in constrained-iterative algorithm. 2D image processing was done in Zen Blue, arrangements and montages were done in FIJI. 3D image processing was done in Arivis 4D (arivis AG); videos were cut and arranged in Adobe Premiere Pro (Adobe Inc.).

BAC Mutagenesis

BAC mutagenesis was performed as described before by en-passant Red Recombination (Tischer et al., 2010). The creation of HCMV-TB40/BAC4-pp150-SNAP-gM-mScarlet-I was done in two steps. At first, UL32 (gene locus of pp150) was mutated by the C-terminal insertion (after K1045) of the SNAP-Tag-SCE-I-KanR shuttle sequence with a nine amino acid linker (HTEDPPVAT) and subsequent second recombination to clear the Kanamycin resistance and restore the SNAP-Tag sequence (complete insertion sequence see Table 1/ REF SNAP-Tag). This was followed up by the insertion of the mScarlet-I (Bindels et al., 2016) sequence in the UL100 gene between the codons for amino acids V62 and M63 of gM by amplifying the mScarlet-I-SCE-I-KanR shuttle construct with the primers shown in Table 2, with the second recombination as described for the first step. The virus was reconstituted by electroporation of the BAC DNA into HFF cells.

Gateway Cloning and Lentivirus Transduction

Plasmid pCMV-Sport6-CD63pHluorin was a gift from DM Pegtel through Addgene (Addgene plasmid # 130601 ; http://n2t.net/addgene:130901 ; RRID:Addgene_130901, Addgene). For Gateway (Thermo Fisher Scientific) cloning, the pCMV-Sport6-CD63pHluorin was recombined with pDONR-221 (Thermo Fisher Scientific) to produce the pENTR-CD63pHluorin vector that was further recombined with pLenti-CMV-Puro-DEST (w118-1), a gift from Eric Campeau & Paul Kaufman through Addgene (Addgene plasmid # 17452; http://n2t.net/addgene:17452; RRID: Addgene_17452).
The resulting pLenti-CMV-CD63pHluorin-Puro was then transfected with polyethyleneimine (Polysciences) together with 3rd generation Lentivirus vector helper plasmids, gifts by Didier Trono, RRID: Addgene_12253, Addgene_12251, Addgene_12259) into 293XT cells (Takara Holdings). Lentivirus containing supernatant was harvested at 48, 72, and 96 hours post-transfection, filtered through 0.2 µm syringe filters and used to transduce HFF-1 cells. 72hpi, the HFF-cells were selected with Puromycin (Thermo Fisher Scientific) at 5 µg/ml. Furthermore, the cells were sorted by fluorescence-activation (FACS), using a FACS Aria Fusion (BD Biosciences), for the 10% strongest fluorescent cells, further cultivated and used for the experiments.

Immunofluorescence

For immunofluorescence experiments, cells were grown in 35mm glass-bottom Ibidi dishes and fixed at the indicated time-points with 4%PFA in D-PBS. SNAP labeling with SNAP-Cell 647-SIR was done as described in the manual for SNAP-Cell 647-SIR (NEB). Afterward, the samples were permeabilized with TritonX-100 at 0.1% in D-PBS with subsequent blocking with 3% Bovine Serum Albumin (Sigma-Aldrich) in D-PBS. Primary antibodies used in this study were Ultra-LEAF™ Purified anti-human CD63 H5C6 (Biolegend), Anti-Cytomegalovirus Glycoprotein B antibody [2F12] (ab6499) (Abcam), Purified anti-human CD9 HI9a (Biolegend), Purified anti-human CD81 (TAPA-1) 5A6 (Biolegend). Secondary antibodies used were Alexa 647 goat anti-mouse (Thermo Fisher Scientific) and Alexa 488 goat anti-mouse (Thermo Fisher Scientific).

Quantification of the frequency of extracellular viral assemblies

HFF-WT cells were infected with HCMV-pp150-SNAP-gM-mScarlet-I or HCMV-TB40-WT at an MOI of 1 and fixed at 120hpi. HCMV-TB40-WT infected cells were stained for gB as described for the other immunofluorescence experiments. Late infected cells were identified in WT-infected cells by a well identifiable gB-positive assembly complex. In the HCMV-pp150-SNAP-gM-mScarlet-I infected cells, late infected cells were identified by three conditions: 1) Well identifiable gM-positive assembly complex. 2) Nuclear signal of pp150-SNAP. 3) Significant pp150-SNAP signal in the assembly complex.

Confocal Scanning Imaging

Confocal Laser Scanning Microscopy was carried out on a Nikon TI2 microscope (Nikon) equipped with an A1 confocal laser scanning unit, a 1.4 NA 60x Plan Apo objective, PMT, and GaAsP detectors, standard 404, 489, 561, and 637 laser lines, and corresponding filter sets. Imaging conditions were optimized for each sample. Scan sizes were adapted to fulfill the criteria for Nyquist-sampling, resulting in a pixel size of 118 nm. The acquisition was done in NIS-Elements, post-processing and image analysis were performed in FIJI.

Weighted Spatial Colocalization Analysis

For the weighted colocalization heatmaps, pixel intensities were calculated, taking into account the absolute intensities in both channels, as well as the ratio between the intensities. The calculation was performed by first normalizing each channel to relative intensity. In the following, the relative intensities of each pixel in both channels a and b were interpreted as a vector$\binom{a}{b}$, describing the vector to the position of that pixel in a classical scatter plot. The length of the vector was then multiplied by $1 - |\sin(\alpha) - \cos(\alpha)|$ while α being the angle between the vector and the x-axis. This multiplication emphasizes pixels where the two colors colocalize with similar relative intensities. The product then was plotted back to the original pixel position in the image resulting in the heatmap shown in the figures. With this strategy, we could put the information of a 2-channel scatter plot back into the image's spatial context.
The Jupyter notebook for this analysis is available on GitHub:
(https://github.com/QuantitativeVirology/2D-Colocalization)

Gradient purification of HCMV

A 15 cm dish of HFF cells was infected with HCMV-TB40-WT at MOI 0.05. Seven dpi, the infected cells were trypsinized and split onto 16x 15 cm dishes of HFF cells. At 7 dpi, the supernatant was harvested and clarified by centrifugation at 1200 xg for 5 min. The virus was pelleted by centrifugation at 14000xg for 1.5 h at 4°C and then resuspended in 1% FBS/PBS overnight on ice. The resuspended virus was centrifuged at 18000xg for 1 min at 4°C to remove large aggregates and then loaded over a continuous gradient made from 15% sodium tartrate with 30% glycerol (w/w) and 35% sodium tartrate (w/w) in 40 mM sodium phosphate pH 7.4 (Talbot and Almeida,

1977). The gradient was made with a Gradient Master (BioComp Instruments) for an SW41 rotor. After centrifugation at 65000xg for 1.5 h at 4°C, the bands were isolated, diluted 10-fold in PBS, and pelleted at 14000xg for 1.5 h at 4°C. The purified virus pellet was resuspended overnight in PBS and then stored at -80°C.

Mass Spectrometry

The purified virus was mixed with 3 volumes of lysis buffer (100 mM Tris, 50 mM DTT, 8 M Urea pH 8.5) and incubated at room temperature for 15 min. Samples were digested using the FASP protocol, employing 30 kDa molecular weight cut-off filter centrifugal units (Amicon, Merck, (Distler et al., 2016)). Briefly, the lysed virus was added to the centrifugal unit and washed with TU buffer (100 mM Tris, 8 M Urea pH 8.5). Next, 8 mM DTT in TU buffer was added and incubated at 56°C for 15 min. After two further washes, 50 mM iodoacetamide (IAA) in TU buffer was added and incubated for 10 minutes at room temperature. The centrifugal units were washed twice, treated again with DTT, washed once further with TU buffer, and twice with 50 mM ammonium bicarbonate solution. MS grade trypsin (Promega) was added in a 1:100 enzyme:protein ratio, and the sample incubated overnight at 37°C. The flow-through containing trypsinized peptides was collected and pooled, and the sample lyophilized with a SpeedVac (Thermo Fisher Scientific). The resulting peptides were enriched with C18 stage tips prepared in-house and eluted with 80% acetonitrile containing 0.5% acetic acid. The samples were dried down by SpeedVac (Thermo Fisher Scientific) and resuspended in 97% water, 3% acetonitrile with 0.1% formic acid, and 10 fmol/µL E. coli digest (Waters Corporation) for analysis by LC-MS/MS.

Peptides resulting from trypsinization were analyzed on a Synapt G2-Si QToF mass spectrometer connected to a NanoAcquity Ultra Performance UPLC system (both Waters Corporation). The data acquisition mode used was mobility enhanced MSE over m/z range 50-2000 with the high energy collisional voltage in the transfer region ramped from 25 to 55 V. Mobile phases used for chromatographic separation were water with 0.1% formic acid (A) and acetonitrile with 0.1% formic acid (B). Samples were desalted using a reverse-phase SYMMETRY C18 trap column (100 Å, 5 µm, 180 µm x 20 mm, Waters Corporation) at a flow rate of 8 µl/min for 2 minutes. Peptides were separated by a linear gradient (0.3 µl/min, 35 °C; 97-60% mobile phase A over 90 minutes) using an Acquity UPLC M-Class Reversed-Phase (1.7 µm Spherical Hybrid, 76 µm x 250 mm, Waters Corporation).

LC-MS data were peak detected and aligned by Progenesis QI for proteomics (Waters Corporation). Proteins were identified by searching against the Human and HCMV proteomes in Uniprot. The database search was performed with the following parameters: mass tolerance was set to software automatic values; enzyme specified as trypsin; up to two missed cleavages; cysteine carbamidomethylation as a fixed modification, with the oxidation of methionine, S/T phosphorylation, and N-terminal acetylation set as variable modifications. Abundances were estimated by Hi3-based quantitation (Silva et al., 2006).
For comparison with the Turner et al., dataset protein accession was converted to UniParc codes.
Raw MS data have been deposited to PRIDE with accession code PXD023444.

Live TIRF Microscopy

For live-cell TIRF imaging, infection experiments were carried out in 35 mm glass-bottom Ibidi dishes. SNAP labeling with SNAP-Cell 647-SIR was done as described in the manual for SNAP-Cell 647-SIR (NEB) before imaging. Microscopy was performed on a Nikon TI equipped for TIRF microscopy and equipped with standard 488, 561, and 640 laser lines, corresponding filter sets, and an incubation chamber with a heating system. The illumination angle was determined experimentally by manually adjusting for TIRF illumination, and image acquisition was performed with NIS-Elements using an ANDOR iXon Ultra 897 EMCCD camera. Live-cell experiments were carried out at 37°C. Intensity measurements in the time courses were done with FIJI by the manual

placing of ROIs. Analysis of the data and visualization in the graphs was performed in GraphPad Prism.

Acknowledgments

We thank Wolfram Brune, Christian Sinzger, and Kerstin Sampaio for their generous gift of viruses HCMV-TB-40-BAC4 HCMV-pp150-EGFP-gM-mCherry and their support.

This study was funded by the Wellcome Trust through a Collaborative Award (209250/Z/17/Z) to KT, KG, and JBB. KG and JBB are funded by the Deutsche Forschungsgemeinschaft (DFG, German Research Foundation) under Germany's Excellence Strategy – EXC 2155 – project number 390874280. We thank the DFG for funding the lattice light sheet system through a large equipment grant to KG and JB, project number 413831413. We thank Zeiss for including us in their lattice light-sheet early adaptor program. FJF is holding a graduate student fellowship by the Studienstiftung des deutschen Volkes. The Leibniz Institute for Experimental Virology is supported by the Free and Hanseatic City of Hamburg and the Federal Ministry of Health. This study is part of the Leibniz ScienceCampus InterACt (Grant Agreement No. W6/2018). The mass spectrometer used in this study was funded by a Wellcome Trust instrumentation grant 104913/Z/14/Z to KT.

Acknowledgments

The authors declare no competing interests.

References

Adler, B. (2015). A Viral Pilot for HCMV Navigation? Viruses *7*, 3857–3862.

Bebelman, M.P., Bun, P., Huveneers, S., Niel, G. van, Pegtel, D.M., and Verweij, F.J. (2020). Real-time imaging of multivesicular body–plasma membrane fusion to quantify exosome release from single cells. Nat Protoc *15*, 102–121.

Bindels, D.S., Haarbosch, L., Weeren, L. van, Postma, M., Wiese, K.E., Mastop, M., Aumonier, S., Gotthard, G., Royant, A., Hink, M.A., et al. (2016). mScarlet: a bright monomeric red fluorescent protein for cellular imaging. Nat Methods *14*, nmeth.4074.

Britt, W.J., and Prichard, M.N. (2018). New therapies for human cytomegalovirus infections. Antivir Res *159*, 153–174.

Bronzini, M., Luganini, A., Dell'Oste, V., Andrea, M.D., Landolfo, S., and Gribaudo, G. (2012). The US16 Gene of Human Cytomegalovirus Is Required for Efficient Viral Infection of Endothelial and Epithelial Cells. J Virol *86*, 6875–6888.

Bughio, F., Elliott, D.A., and Goodrum, F. (2013). An Endothelial Cell-Specific Requirement for the UL133-UL138 Locus of Human Cytomegalovirus for Efficient Virus Maturation. J Virol *87*, 3062–3075.

Bughio, F., Umashankar, M., Wilson, J., and Goodrum, F. (2015). Human Cytomegalovirus UL135 and UL136 Genes Are Required for Postentry Tropism in Endothelial Cells. J Virol *89*, 6536–6550.

Butt, B.G., Owen, D.J., Jeffries, C.M., Ivanova, L., Hill, C.H., Houghton, J.W., Ahmed, M.F., Antrobus, R., Svergun, D.I., Welch, J.W., et al. (2020). Insights into herpesvirus assembly from the structure of the pUL7:pUL51 complex. Elife *9*, e53789.

Calistri, A., Sette, P., Salata, C., Cancellotti, E., Forghieri, C., Comin, A., Göttlinger, H., Campadelli-Fiume, G., Palù, G., and Parolin, C. (2007). Intracellular Trafficking and Maturation of Herpes Simplex Virus Type 1 gB and Virus Egress Require Functional Biogenesis of Multivesicular Bodies ▿. J Virol *81*, 11468–11478.

628 Cepeda, V., Esteban, M., and Fraile- Ramos, A. (2010). Human cytomegalovirus final
629 envelopment on membranes containing both trans- Golgi network and endosomal markers. Cell
630 Microbiol *12*, 386–404.
631 Cocucci, E., Racchetti, G., and Meldolesi, J. (2009). Shedding microvesicles: artefacts no more.
632 Trends Cell Biol *19*, 43–51.
633 Colombo, M., Raposo, G., and Théry, C. (2014). Biogenesis, Secretion, and Intercellular
634 Interactions of Exosomes and Other Extracellular Vesicles. Annu Rev Cell Dev Bi *30*, 1–35.
635 Crump, C.M., Yates, C., and Minson, T. (2007). Herpes Simplex Virus Type 1 Cytoplasmic
636 Envelopment Requires Functional Vps4 ▿. J Virol *81*, 7380–7387.
637 Das, S., and Pellett, P.E. (2011). Spatial Relationships between Markers for Secretory and
638 Endosomal Machinery in Human Cytomegalovirus-Infected Cells versus Those in Uninfected
639 Cells. J Virol *85*, 5864–5879.
640 Das, S., Vasanji, A., and Pellett, P.E. (2007). Three-Dimensional Structure of the Human
641 Cytomegalovirus Cytoplasmic Virion Assembly Complex Includes a Reoriented Secretory
642 Apparatus ▿ †. J Virol *81*, 11861–11869.
643 Dietz, A.N., Villinger, C., Becker, S., Frick, M., and Einem, J. von (2018). A Tyrosine-Based
644 Trafficking Motif of the Tegument Protein pUL71 Is Crucial for Human Cytomegalovirus
645 Secondary Envelopment. J Virol *92*, e00907-17.
646 Distler, U., Kuharev, J., Navarro, P., and Tenzer, S. (2016). Label-free quantification in ion
647 mobility–enhanced data-independent acquisition proteomics. Nat Protoc *11*, 795–812.
648 Dogrammatzis, C., Deschamps, T., and Kalamvoki, M. (2018). Biogenesis of extracellular
649 vesicles during herpes simplex virus type 1 infection: The role of the CD63 tetraspanin. J Virol *93*,
650 JVI.01850-18.
651 Fraile- Ramos, A., Pelchen- Matthews, A., Risco, C., Rejas, M.T., Emery, V.C., Hassan- Walker,
652 A.F., Esteban, M., and Marsh, M. (2007). The ESCRT machinery is not required for human
653 cytomegalovirus envelopment. Cell Microbiol *9*, 2955–2967.
654 Griffiths, P. (2020). The direct and indirect consequences of cytomegalovirus infection and
655 potential benefits of vaccination. Antivir Res *176*, 104732.
656 Hashimoto, Y., Sheng, X., Murray-Nerger, L.A., and Cristea, I.M. (2020). Temporal dynamics of
657 protein complex formation and dissociation during human cytomegalovirus infection. Nat
658 Commun *11*, 806.
659 Hogue, I.B. (2022). Tegument Assembly, Secondary Envelopment and Exocytosis. Curr Issues
660 Mol Biol *42*, 551–604.
661 Hogue, I.B., Bosse, J.B., Hu, J.-R., Thiberge, S.Y., and Enquist, L.W. (2014). Cellular
662 Mechanisms of Alpha Herpesvirus Egress: Live Cell Fluorescence Microscopy of Pseudorabies
663 Virus Exocytosis. Plos Pathog *10*, e1004535.
664 Hogue, I.B., Scherer, J., and Enquist, L.W. (2016). Exocytosis of Alphaherpesvirus Virions, Light
665 Particles, and Glycoproteins Uses Constitutive Secretory Mechanisms. Mbio *7*, e00820-16.
666 Hollinshead, M., Johns, H.L., Sayers, C.L., Gonzalez- Lopez, C., Smith, G.L., and Elliott, G.
667 (2012). Endocytic tubules regulated by Rab GTPases 5 and 11 are used for envelopment of
668 herpes simplex virus. Embo J *31*, 4204–4220.
669 Homman-Loudiyi, M., Hultenby, K., Britt, W., and Söderberg-Nauclér, C. (2003). Envelopment of
670 Human Cytomegalovirus Occurs by Budding into Golgi-Derived Vacuole Compartments Positive
671 for gB, Rab 3, Trans-Golgi Network 46, and Mannosidase II. J Virol *77*, 3191–3203.
672 Johnson, D.C., and Baines, J.D. (2011). Herpesviruses remodel host membranes for virus
673 egress. Nat Rev Microbiol *9*, 382–394.
674 Kharkwal, H., Smith, C.G., and Wilson, D.W. (2014). Blocking ESCRT-Mediated Envelopment
675 Inhibits Microtubule-Dependent Trafficking of Alphaherpesviruses In Vitro. J Virol *88*, 14467–
676 14478.
677 Kosaka, N., Iguchi, H., Yoshioka, Y., Takeshita, F., Matsuki, Y., and Ochiya, T. (2010). Secretory
678 Mechanisms and Intercellular Transfer of MicroRNAs in Living Cells. J Biol Chem *285*, 17442–
679 17452.

Li, G., Nguyen, C.C., Ryckman, B.J., Britt, W.J., and Kamil, J.P. (2015). A viral regulator of glycoprotein complexes contributes to human cytomegalovirus cell tropism. Proc National Acad Sci *112*, 4471–4476.

Luganini, A., Cavaletto, N., Raimondo, S., Geuna, S., and Gribaudo, G. (2017). Loss of the Human Cytomegalovirus US16 Protein Abrogates Virus Entry into Endothelial and Epithelial Cells by Reducing the Virion Content of the Pentamer. J Virol *91*, e00205-17.

Maninger, S., Bosse, J.B., Lemnitzer, F., Pogoda, M., Mohr, C.A., Einem, J. von, Walther, P., Koszinowski, U.H., and Ruzsics, Z. (2011). M94 Is Essential for the Secondary Envelopment of Murine Cytomegalovirus ‡. J Virol *85*, 9254–9267.

Meissner, C.S., Suffner, S., Schauflinger, M., Einem, J. von, and Bogner, E. (2012). A Leucine Zipper Motif of a Tegument Protein Triggers Final Envelopment of Human Cytomegalovirus. J Virol *86*, 3370–3382.

Mingo, R.M., Han, J., Newcomb, W.W., and Brown, J.C. (2012). Replication of Herpes Simplex Virus: Egress of Progeny Virus at Specialized Cell Membrane Sites. J Virol *86*, 7084–7097.

Modlin, J.F., Arvin, A.M., Fast, P., Myers, M., Plotkin, S., and Rabinovich, R. (2004). Vaccine Development to Prevent Cytomegalovirus Disease: Report from the National Vaccine Advisory Committee. Clin Infect Dis *39*, 233–239.

Momtaz, S., Molina, B., Mlera, L., Goodrum, F., and Wilson, J.M. (2021). Cell type-specific biogenesis of novel vesicles containing viral products in human cytomegalovirus infection. J Virol.

Moorman, N.J., Sharon-Friling, R., Shenk, T., and Cristea, I.M. (2010). A Targeted Spatial-Temporal Proteomics Approach Implicates Multiple Cellular Trafficking Pathways in Human Cytomegalovirus Virion Maturation. Mol Cell Proteomics *9*, 851–860.

Mori, Y., Koike, M., Moriishi, E., Kawabata, A., Tang, H., Oyaizu, H., Uchiyama, Y., and Yamanishi, K. (2008). Human Herpesvirus- 6 Induces MVB Formation, and Virus Egress Occurs by an Exosomal Release Pathway. Traffic *9*, 1728–1742.

Nguyen, C.C., Siddiquey, M.N.A., Zhang, H., Li, G., and Kamil, J.P. (2018). Human Cytomegalovirus Tropism Modulator UL148 Interacts with SEL1L, a Cellular Factor That Governs Endoplasmic Reticulum-Associated Degradation of the Viral Envelope Glycoprotein gO. J Virol *92*, e00688-18.

Owen, D.J., Crump, C.M., and Graham, S.C. (2015). Tegument Assembly and Secondary Envelopment of Alphaherpesviruses. Viruses *7*, 5084–5114.

Pawliczek, T., and Crump, C.M. (2009). Herpes Simplex Virus Type 1 Production Requires a Functional ESCRT-III Complex but Is Independent of TSG101 and ALIX Expression ▿. J Virol *83*, 11254–11264.

Perez-Hernandez, D., Gutiérrez-Vázquez, C., Jorge, I., López-Martín, S., Ursa, A., Sánchez-Madrid, F., Vázquez, J., and Yáñez-Mó, M. (2013). The Intracellular Interactome of Tetraspanin-enriched Microdomains Reveals Their Function as Sorting Machineries toward Exosomes. J Biol Chem *288*, 11649–11661.

Procter, D.J., Banerjee, A., Nukui, M., Kruse, K., Gaponenko, V., Murphy, E.A., Komarova, Y., and Walsh, D. (2018). The HCMV Assembly Compartment Is a Dynamic Golgi-Derived MTOC that Controls Nuclear Rotation and Virus Spread. Dev Cell *45*, 83-100.e7.

Radsak, K., Eickmann, M., Mockenhaupt, T., Bogner, E., Kern, H., Eis-Hübinger, A., and Reschke, M. (1996). Retrieval of human cytomegalovirus glycoprotein B from the infected cell surface for virus envelopment. Arch Virol *141*, 557–572.

Sampaio, K., Jahn, G., and Sinzger, C. (2013). Virus-Host Interactions, Methods and Protocols. Methods Mol Biology Clifton N J *1064*, 201–209.

Sanchez, V., Greis, K.D., Sztul, E., and Britt, W.J. (2000). Accumulation of Virion Tegument and Envelope Proteins in a Stable Cytoplasmic Compartment during Human Cytomegalovirus Replication: Characterization of a Potential Site of Virus Assembly. J Virol *74*, 975–986.

Schauflinger, M., Fischer, D., Schreiber, A., Chevillotte, M., Walther, P., Mertens, T., and Einem, J. von (2011). The Tegument Protein UL71 of Human Cytomegalovirus Is Involved in Late Envelopment and Affects Multivesicular Bodies. J Virol *85*, 3821–3832.

Schauflinger, M., Villinger, C., Mertens, T., Walther, P., and Einem, J. (2013). Analysis of human cytomegalovirus secondary envelopment by advanced electron microscopy. Cell Microbiol *15*, 305–314.

Scrivano, L., Sinzger, C., Nitschko, H., Koszinowski, U.H., and Adler, B. (2011). HCMV Spread and Cell Tropism are Determined by Distinct Virus Populations. Plos Pathog *7*, e1001256.

Silva, J.C., Gorenstein, M.V., Li, G.-Z., Vissers, J.P.C., and Geromanos, S.J. (2006). Absolute Quantification of Proteins by LCMSE A Virtue of Parallel ms Acquisition. Mol Cell Proteomics *5*, 144–156.

Sinzger, C., Hahn, G., Digel, M., Katona, R., Sampaio, K.L., Messerle, M., Hengel, H., Koszinowski, U., Brune, W., and Adler, B. (2008). Cloning and sequencing of a highly productive, endotheliotropic virus strain derived from human cytomegalovirus TB40/E. J Gen Virol *89*, 359–368.

Streck, N.T., Carmichael, J., and Buchkovich, N.J. (2018). Nonenvelopment Role for the ESCRT-III Complex during Human Cytomegalovirus Infection. J Virol *92*, e02096-17.

Streck, N.T., Zhao, Y., Sundstrom, J.M., and Buchkovich, N.J. (2020). Human Cytomegalovirus Utilizes Extracellular Vesicles to Enhance Virus Spread. J Virol.

Taisne, C., Lussignol, M., Hernandez, E., Moris, A., Mouna, L., and Esclatine, A. (2019). Human cytomegalovirus hijacks the autophagic machinery and LC3 homologs in order to optimize cytoplasmic envelopment of mature infectious particles. Sci Rep-Uk *9*, 4560.

Takino, T., Miyamori, H., Kawaguchi, N., Uekita, T., Seiki, M., and Sato, H. (2003). Tetraspanin CD63 promotes targeting and lysosomal proteolysis of membrane-type 1 matrix metalloproteinase. Biochem Bioph Res Co *304*, 160–166.

Talbot, P., and Almeida, J.D. (1977). Human Cytomegalovirus: Purification of Enveloped Virions and Dense Bodies. J Gen Virol *36*, 345–349.

Tandon, R., AuCoin, D.P., and Mocarski, E.S. (2009). Human Cytomegalovirus Exploits ESCRT Machinery in the Process of Virion Maturation ▿. J Virol *83*, 10797–10807.

Théry, C., Zitvogel, L., and Amigorena, S. (2002). Exosomes: composition, biogenesis and function. Nat Rev Immunol *2*, 569–579.

Tischer, B.K., Smith, G.A., and Osterrieder, N. (2010). In Vitro Mutagenesis Protocols, Third Edition. 421–430.

Tooze, J., Hollinshead, M., Reis, B., Radsak, K., and Kern, H. (1993). Progeny vaccinia and human cytomegalovirus particles utilize early endosomal cisternae for their envelopes. Eur J Cell Biol *60*, 163–178.

Tugizov, S., Maidji, E., Xiao, J., and Pereira, L. (1999). An Acidic Cluster in the Cytosolic Domain of Human Cytomegalovirus Glycoprotein B Is a Signal for Endocytosis from the Plasma Membrane. J Virol *73*, 8677–8688.

Turner, D.L., Korneev, D.V., Purdy, J.G., Marco, A. de, and Mathias, R.A. (2020). The host exosome pathway underpins biogenesis of the human cytomegalovirus virion. Elife *9*, e58288.

van Niel, G., Charrin, S., Simoes, S., Romao, M., Rochin, L., Saftig, P., Marks, M.S., Rubinstein, E., and Raposo, G. (2011). The Tetraspanin CD63 Regulates ESCRT-Independent and -Dependent Endosomal Sorting during Melanogenesis. Dev Cell *21*, 708–721.

Varnum, S.M., Streblow, D.N., Monroe, M.E., Smith, P., Auberry, K.J., Paša-Tolić, L., Wang, D., Camp, D.G., Rodland, K., Wiley, S., et al. (2004). Identification of Proteins in Human Cytomegalovirus (HCMV) Particles: the HCMV Proteome. J Virol *78*, 10960–10966.

Walton, J. (1979). Lead asparate, an en bloc contrast stain particularly useful for ultrastructural enzymology. J Histochem Cytochem Official J Histochem Soc *27*, 1337–1342.

Yáñez-Mó, M., Barreiro, O., Gordon-Alonso, M., Sala-Valdés, M., and Sánchez-Madrid, F. (2009). Tetraspanin-enriched microdomains: a functional unit in cell plasma membranes. Trends Cell Biol *19*, 434–446.

Zicari, S., Arakelyan, A., Palomino, R.A.Ñ., Fitzgerald, W., Vanpouille, C., Lebedeva, A., Schmitt, A., Bomsel, M., Britt, W., and Margolis, L. (2018). Human cytomegalovirus-infected cells release extracellular vesicles that carry viral surface proteins. Virology *524*, 97–105.

786

Figures and Tables

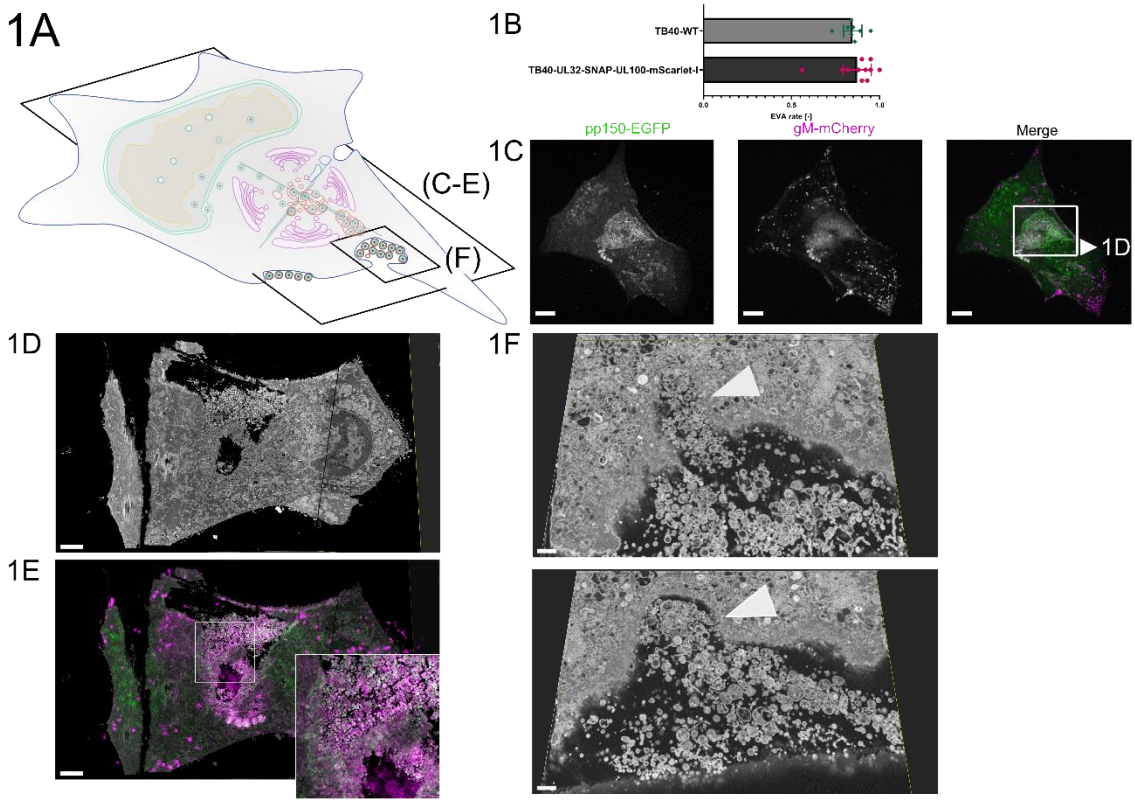

Figure 1. Large EVAs contain viral products and other vesicular material. CLEM of HFF cells infected with HCMV-pp150-EGFP-gM-mCherry (MOI 3) at 4 dpi. **1A** Overview scheme indicating the positions of the panels in relation to the whole cell. **1B** Quantification of EVA occurrence. HFF-WT cells were infected with HCMV-pp150-SNAP-gM-mScarlet-I or HCMV-TB40-WT at an MOI of 1 and fixed at 120hpi. HCMV-TB40-WT infected cells were stained for gB. Late-infected cells were counted and the rate of EVAs was quantified. Borders show the 95% confidence interval of the mean. N=269 from 11 replicates for HCMV-pp150-SNAP-gM-mScarlet-I and N=750 from 8 replicates for HCMV-TB40-WT. **1C** Spinning-disk confocal section of pp150-EGFP (pp150EGFP) and gM-mCherry (gMmCherry) signal close to the plasma membrane. Large accumulations of virus particles, marked by the white frame, are located below the cell. Scale bar represents 10 µm. **1D** SBF-SEM images and **1E** correlation to fluorescence data for the area below the cell, confirming that EVAs are located outside of the cell. Scale bar represents 3 µm. **1F** Two details of z-slices depicting invaginations (white arrowheads) that can be found in SBF-SEM data occurring along the cell surface. Scale bars represent 700 nm.

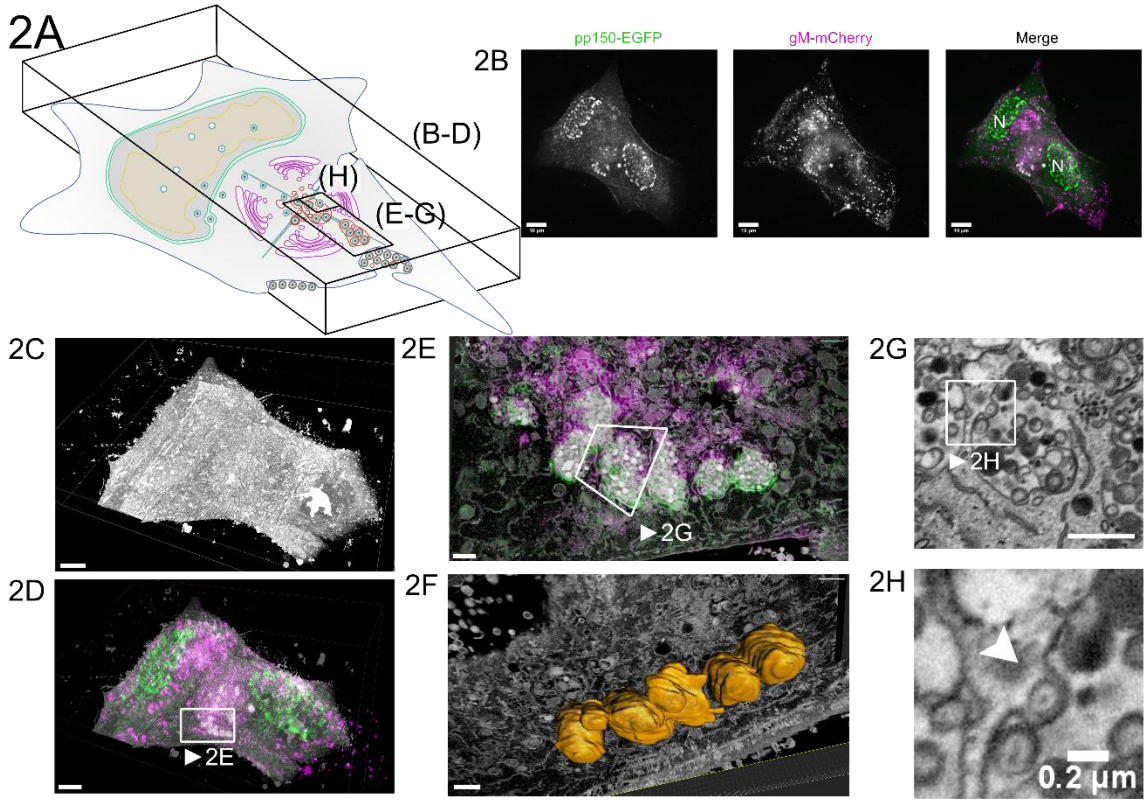

Figure 2 Correlative fluorescence and EM data show large multivesicular bodies filled with virus progeny. 2A Overview scheme indicating the positions of the panels in relation to the whole cell. CLEM of HFF-cells infected with HCMV-pp150-EGFP-gM-mCherry (MOI 3) at 4dpi. **2B** Maximum z-projection of a 3D spinning-disk confocal microscopy stack. pp150-EGFP is colored in green and gM-mCherry signal in magenta. In the merged channel image (Merge), N marks nuclei, containing pp150 signal. Scale bar indicates 10 µm. **2C** 3D rendering of the SBF-SEM data corresponding to the cell shown in 1A. **2D** Correlative overlay of merged channels from 2B and 2C. The white frame marks MVBs that are also highlighted in 2E-F and Sup. Vid. 1B. Scale bar indicates 7 µm. **2E** Rendering of SBF-SEM data marked in 2D correlated with 3-dimensional fluorescence data. **2F** Exemplary surface renderings showing the largest bodies in the field of view. Scale bars indicates 1 µm**. 2G** Enlarged excerpt from the SBF-SEM dataset shown in 2C. The signal is inverted to facilitate comparison with TEM images. Also, refer to Sup. Vid. 1A-B for a 3D rendering of the presented data. Scale bar indicates 1 µm. **2H** Detail from 2G marked with the white frame. Scale bar indicates 0.2 µm.

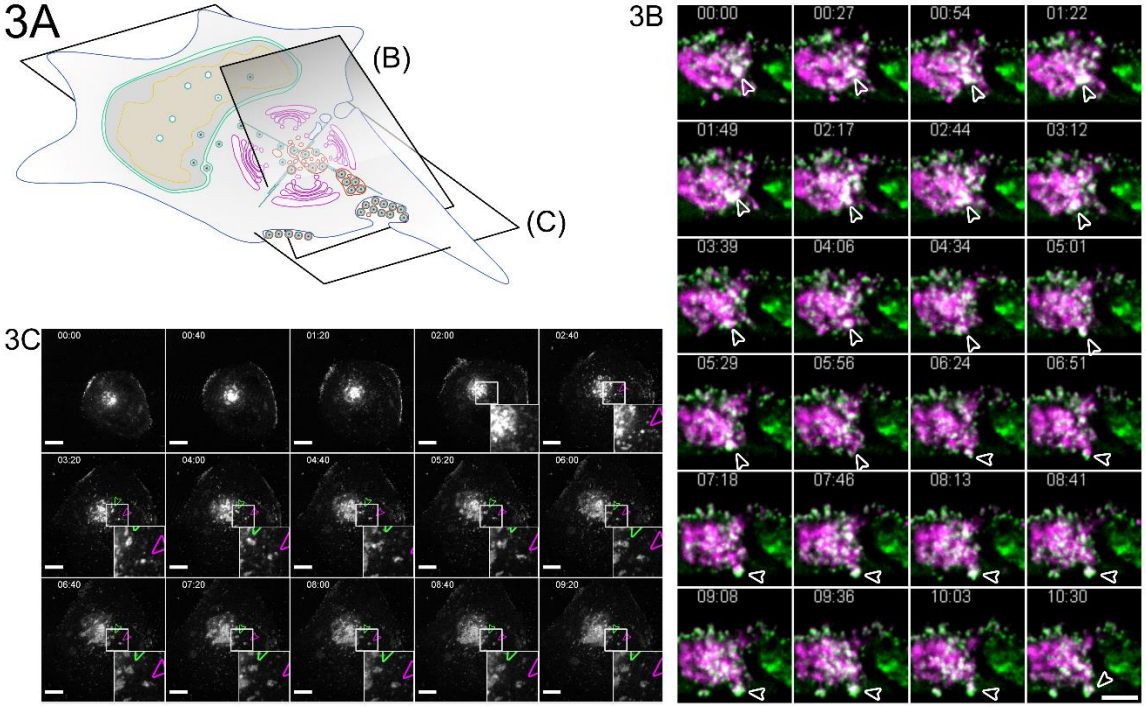

Figure 3. Bulk release from vMVBs leads to EVA formation. 3A Overview scheme indicating the positions of the panels in relation to the whole cell. **3B** HFF cells were infected with HCMV-pp150EGFP-gM-mCherry at an MOI of 1. At 96 hpi the cells were imaged by lattice light-sheet microscopy, taking volumes of whole cells every 2.11 seconds. Shown is a montage of time-lapse images of a single plane at a 30° angle to the growth substrate. Indicated with the white arrowhead is a large body that approaches the plasma membrane and relaxes at it. Scale bar indicates 5 µm. Time format is mm:ss. Also, refer to Sup. Vid. 2 for a rendering and several side views. **3C** HFF cells were infected with HCMV-pp150-SNAP-gM-mScalet-I at an MOI of 1. At 72 hpi, cells were imaged live with confocal spinning disk microscopy. EVAs are highlighted with colored arrowheads. Scale bar indicates 10 µm. The time format is hh:mm. Also, refer to Sup. Vid. 3 and 4.

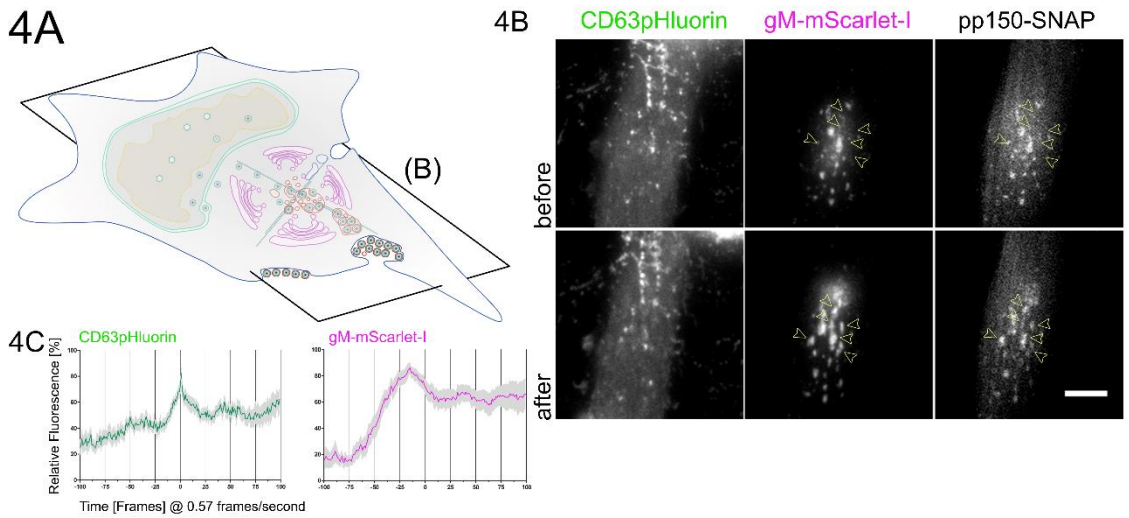

Figure 4. EVAs are the result of fusion events between vMVBs and the plasma membrane. **4A** Overview scheme indicating the positions of the panels in relation to the whole cell. HFF-CD63pHluorin were infected with HCMV-pp150-SNAP-gM-mScarlet-I and imaged at 72 and 96 hpi by fluorescence microscopy in TIRF conditions over 1 hour at an average frame rate of 0.57 frames per second (fps). **4B** TIRF images of a cell before (before) and after (after) bulk release events from vMVBs occurred. Positions of EVA formation are marked by arrows. **4C** Quantification of EVA formation events. Solid lines are averages from 14 events extracted from 5 cells in 4 replicates. Grey areas show the standard error of the mean. Scale bar indicates 10 µm.

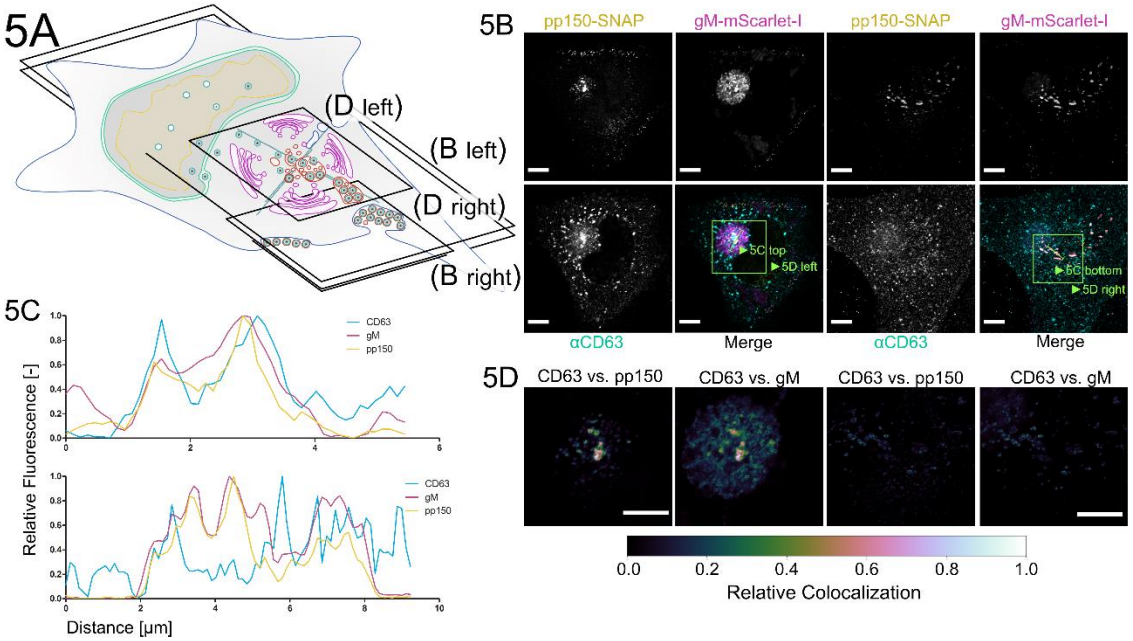

Figure 5. Tetraspanin CD63 colocalizes to vMVBs containing with gM and pp150. 5A Overview scheme indicating the positions of the subfigures in relation to the whole cell. **5B** HFF-WT cells were infected at an MOI of 1 with HCMV-pp150-SNAP-gM-mScarlet-I, fixed at 4 dpi, stained for CD63 and imaged using confocal laser scanning microscopy. A representative cell is shown at two z-heights. The four images on the left show the center of the cell, the images on the right show the plasma membrane at the cover glass. The localization pattern of CD63 (αCD63) was compared to gM (gM-mScarlet-I), and pp150 (pp150-SNAP). In the center of the cell, CD63 localized to the assembly complex center and marked vMVBs in the cytoplasm that are pp150 and gM positive. At the plasma membrane EVAs are positive for pp150 and gM signals but lack CD63. **5C** Line plots for the indicated areas in 5B. **5D** Spatially weighted colocalization analysis shows areas in the assembly complex where CD63 colocalization with vMVBs is especially pronounced (left two images). No significant colocalization between CD63 and pp150 or gM is present in EVAs. All scale bars indicate 10 µm.

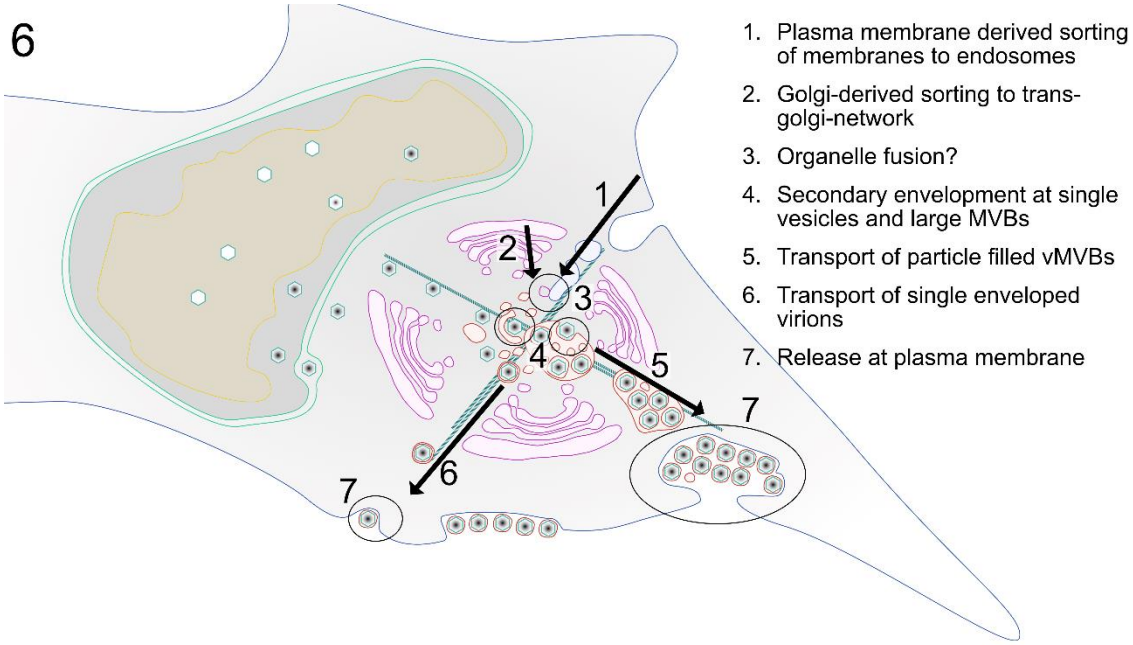

Figure 6. Scheme of possible HCMV release pathways. 1-3 Membranes of late-endosomal and trans-Golgi origin are trafficked to the assembly complex and subsequently utilized for secondary envelopment. **4** Capsids egress from the nucleus and are trafficked to the assembly complex where they either bud individually into single vesicles or into vMVBs. **5-6** Vesicles and MVBs are transported towards the plasma membrane and **7** fuse with it to release their content to the extracellular space potentially as divergent egress pathways.

875 **Table 1. Sequences for 2-Step BAC mutagenesis of HCMV-TB40-pp150-SNAP-gM-**
876 **mScarlet-I.**
877

TB40-pp150-SNAP Insert Sequence	
Insert Sequence	**CACACGGAGGATCCACCGGTCGCCACC atggacaaagactgcgaaatgaagcgcaccaccctg gatagccctctgggcaagctggaactgtctgggtgcg aacagggcctgcacgagatcaagctgctgggcaaag gaacatctgccgccgacgccgtggaagtgcctgcccc agccgccgtgctgggcggaccagagccactgatgca ggccaccgcctggctcaacgcctactttcaccagcctg aggccatcgaggagttccctgtgccagccctgcaccac ccagtgttccagcaggagagctttacccgccaggtgct gtggaaactgctgaaagtggtgaagttcggagaggtca tcagctaccagcagctggccgccctggccggcaatcc cgccgccaccgccgccgtgaaaaccgccctgagcgg aaatcccgtgcccattctgatcccctgccaccgggtggt gtctagctctggcgccgtgggggctacgagggcggg ctcgccgtgaaagagtggctgctggcccacgagggcc acagactgggcaagcctgggctgggt**
TB40-gM-mScarlet-I Primer (50bp overhangs)	
Forward	**ACT ATC ACG TCG TGG ACT TTG AAA GGC TCA ACA TGT CGG CCT ACA ACG TAG TGA GCA AGG GCG AGG C**
Reverse	**CAC ACC AGC TGC ACC GAG TCT AAG AAA AGC ATA GGC GTG TGC AGG TGC ATC TTG TAC AGC TCG TCC ATG CC**

878
879
880

Supplementary Figure 1

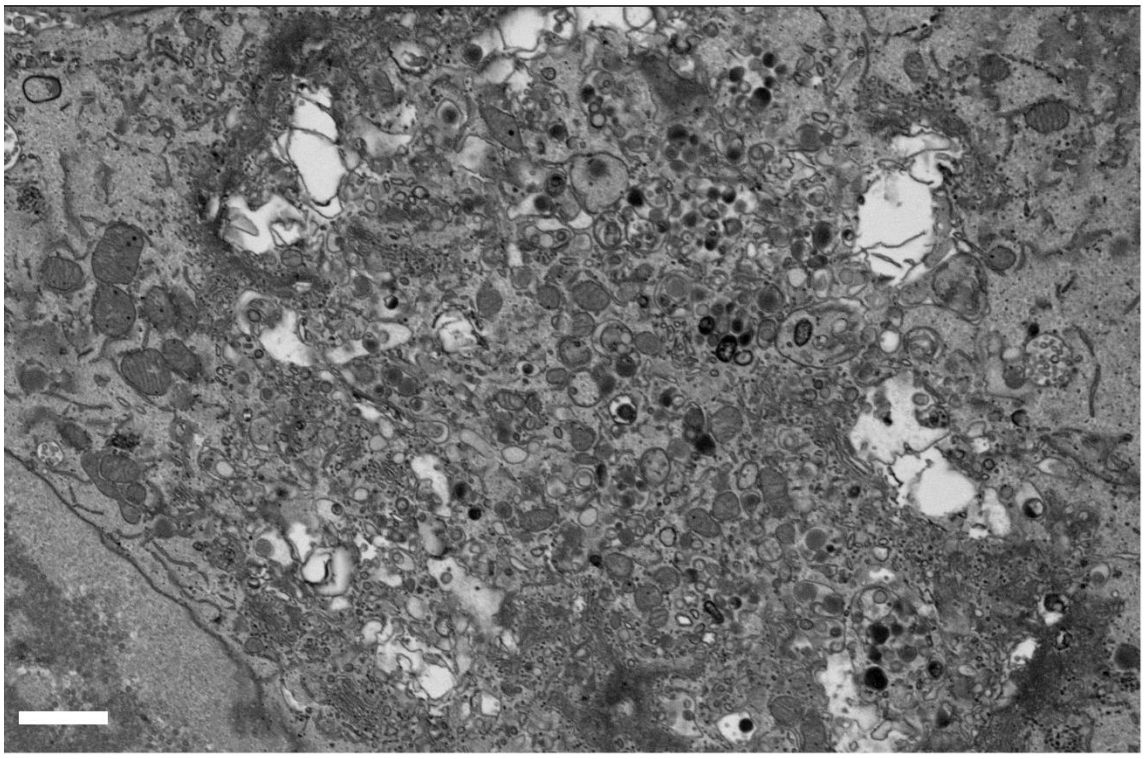

Supplementary Figure 1. A Resliced overview of an HCMV assembly complex in an infected HFF cell. HFF-WT cell infected with HCMV-pp150-EGFP-gM-mCherry (MOI 3) at 4dpi. Shown is the assembly complex in a resliced section through an SBFSEM stack. Scale bar indicates 1.5 µm.

Supplementary Figure 2

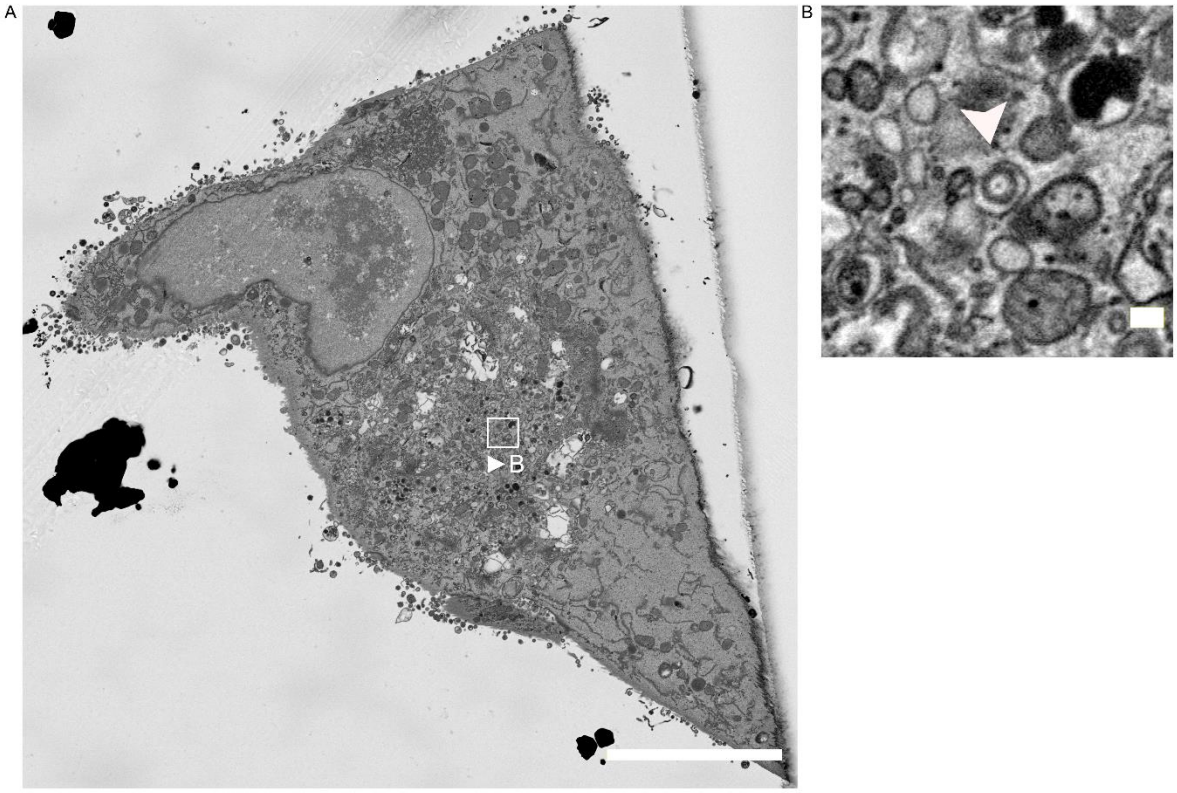

886

887 **Supplementary Figure 2.** **S2A** Single SBF-SEM section of an infected HFF cell. HFF-WT cell
888 infected with HCMV-pp150-EGFP-gM-mCherry (MOI 3) at 4dpi. The white frame indicates the area
889 cropped and enlarged in B. Scale bar indicates 10 µm. **S2B** A detail showing a single capsid
890 budding into a single vesicle (white arrowhead). Scale bar indicates 200nm.

891

Supplementary Figure 3

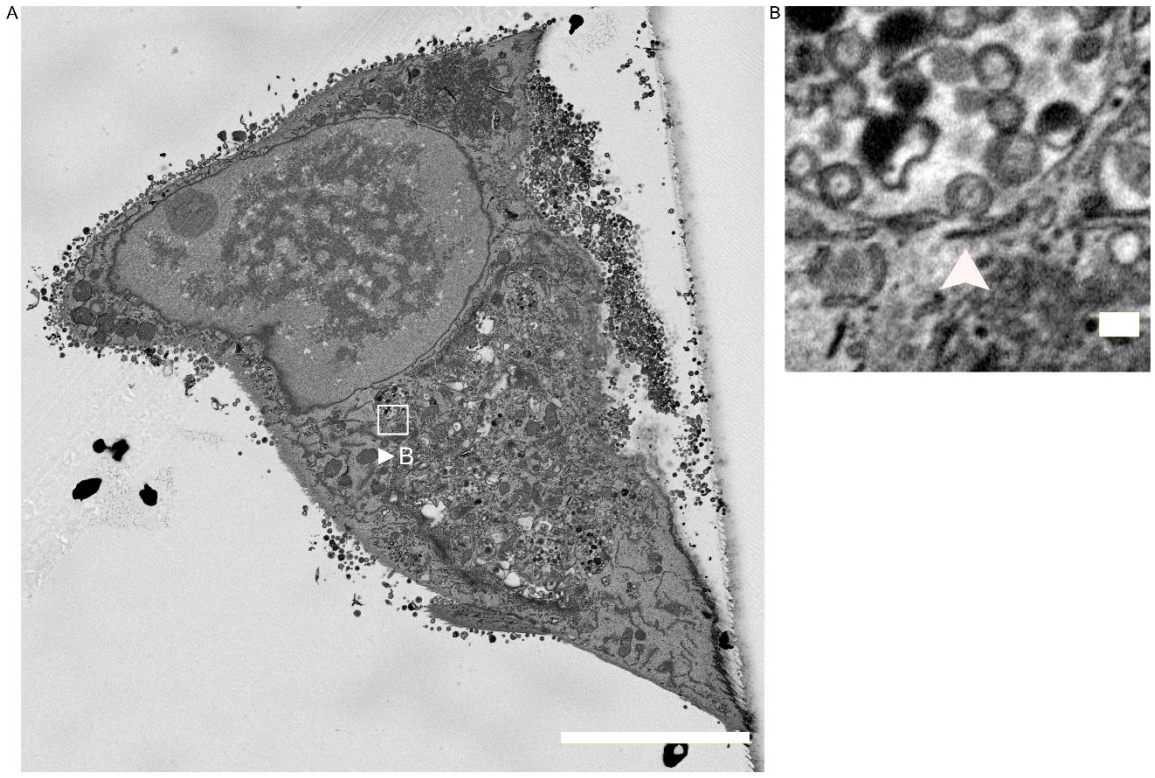

892

893 **Supplementary Figure 3.** **S3A** Single SBF-SEM section of an infected HFF cell. HFF-WT cell
894 infected with HCMV-pp150-EGFP-gM-mCherry (MOI 3) at 4dpi. The white frame indicates the area
895 cropped and enlarged in B. Scale bar indicates 10 µm. **S3B** A detail showing a single particle
896 budding into a vMVB (white arrowhead). Scale bar indicates 200nm.

897

898

Supplementary Figure 4

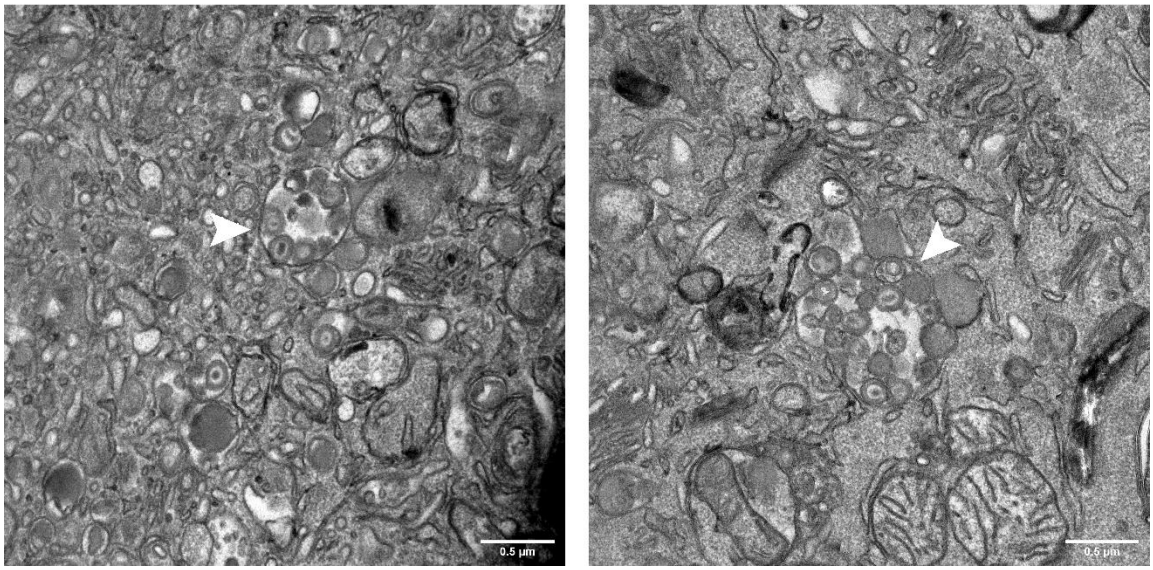

899
900 **Supplementary Figure 4. vMVBs with viral products are not an artifact of fluorescent protein**
901 **tagging.** HFF-WT cells were infected with HCMV-TB40-WT at an MOI of 5, fixed, and processed
902 for EM as described for SBF-SEM at 120 hpi with the modification that instead of the conductive
903 epon, used for SBF-SEM, the cells were embedded for classical sectioning. vMVBs filled with virus
904 progeny are indicated by filled arrowheads. All scale bars represent 0.5 µm.

905

Supplementary Figure 5

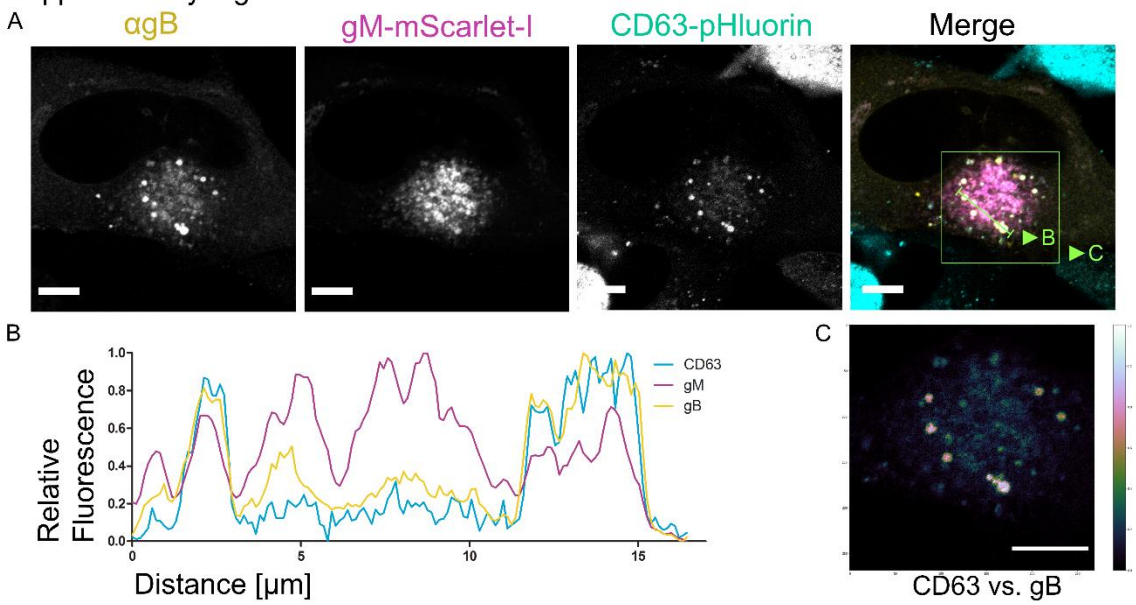

Supplementary Figure 5. Tetraspanin CD63 colocalizes with gM, gB S5A HFF-CD63pHluorin cells were infected at an MOI of 1 with HCMV-pp150-SNAP-gM-mScarlet-I. Cells were fixed at 4 dpi and stained for gB. The images show a representative cell and the localization pattern of CD63 compared to gB and gM. CD63 localizes to large vesicles positive for gB and gM. Scale bars indicate 10 µm. **S5B** Line plot for the indicated areas in A. CD63 signal correlates with gM and gB signals. **S5C** Spatial weighted colocalization analysis highlights the specific areas for CD63 and gB colocalization. Scale bar indicates 10 µm.

Supplementary Figure 6

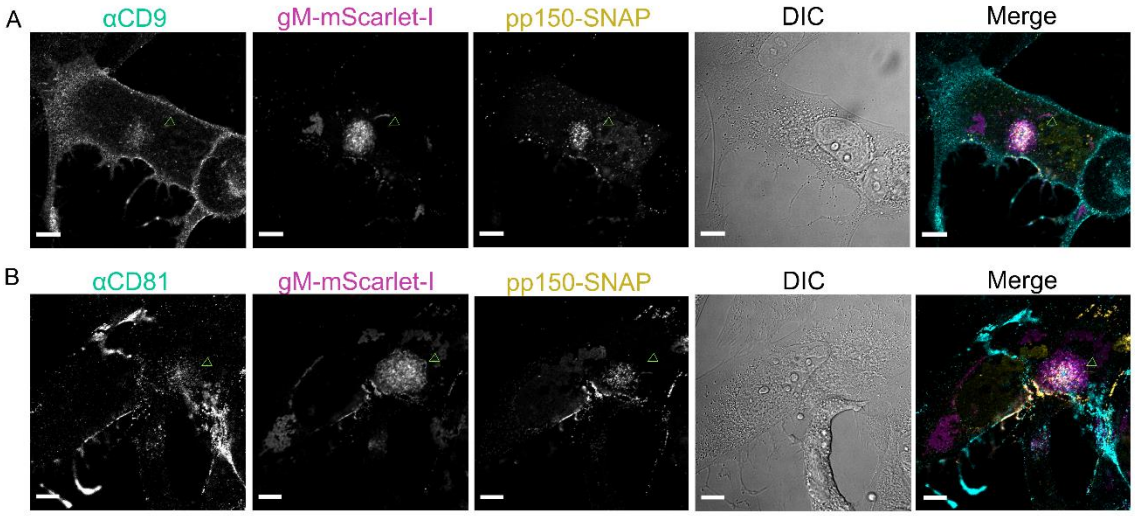

Supplementary Figure 6. Tetraspanins CD9 and CD81 localize to the assembly compartment. S6A-B HFF cells were infected at an MOI of 1 with HCMV-pp150-SNAP-gM-mScarlet-I. Cells were fixed at 4 dpi and stained for CD9 (αCD69) and CD81 (αCD81) using specific antibodies. The images show representative cells and the localization pattern of the CD molecules relative to gM (gM-mScarlet-I) and pp150 (pp150-SNAP) Scale bars indicate 10 µm.

924 **Supplementary Video 1. SBF-SEM of an area between the cell surface and the growth**
925 **substrate.** The video shows a subset of planes from the dataset described in Figure 1 rendered
926 as a video. Infection conditions are as described before. The signal was inverted to resemble TEM
927 contrast. Shown is a large invagination below the cell at the growth substrate.

928

929 **Supplementary Videos 2A and 2B. SBF-SEM rendering of infected HFF cells.** The video shows
930 an excerpt from the dataset described in Figure 1. HFF cells were infected with an MOI of 3 and
931 fixed 4dpi. **2A** Overview rendering of the whole SBF-SEM dataset of the cells shown in Figure 1
932 and 2. **2B** A group of prominent virus-filled MVBs is highlighted by a surface rendering. Several
933 more MVBs are present in the cell.

Supplementary Video 3. Multi-perspective 3D rendering of volumetric time-lapse microscopy data of HCMV release. HFF cell, infected with HCMV-pp150-EGFP-gM-mCherry as described in Figure 3A. The video shows several perspectives how a large vMVB positive for pp150-EGFP (green) and gM-mCherry (red) traverses the cytoplasm and fuses with the plasma membrane. The first seconds show the 3D video, followed by a split-screen part of three different perspectives. A spotlight effect (circle) highlights the same body in all three parts. In the left third, the vMVB is followed by a moving section, parallel to the growth substrate, through the volume on its way downwards to the lower cell surface. In the middle part, the body is followed as a 3D rendering through the cell. The camera angle moves to keep the body visible as well as possible. The last third shows how the vMVB fuses with the plasma membrane in a static cross-section. Due to the optical setup of the lattice-light-sheet microscope (See Figure 3A), the grid added by Arivis 4D (Arivis AG, Rostock, Germany) is tilted 30° respective to the real physical orientation of the cell in the microscope.

Supplementary Videos 4 and 5. Live-cell long time-lapse spinning-disc microscopy videos. HFF cells were infected with HCMV-pp150-SNAP-gM-mScarlet-I at an MOI of 1. At 72 hpi, cells were stained for pp150-SNAP and imaged live by spinning disk microscopy. 8-micrometer stacks in 1-micrometer increments were acquired every 40 minutes. The plane shown is the section of the cell closest to the coverglass. Cells can be seen to release virus particles in short intermittent bursts over several hours, indicated by the white arrowheads. pp150-SNAP labeling is shown in green and gM-mScarlet-I label in magenta. The time format is hh:mm.

958 **Supplementary Table 1** Mass Spectrometry Results.

959